Passive Radar Imaging

Marco Martorella, Fabrizio Berizzi

Department of Information Engineering

University of Pisa

Via Caruso 16, 56122 Pisa, Italy

m.martorella@iet.unipi.it, f.berizzi@iet.unipi.it

ABSTRACT

Passive radar not only offers the ability to exploit illuminators of opportunity to enable radar detection and tracking but also imaging. In these notes, the principles of passive radar imaging are illustrated. This paper is to be considered as companion notes for the NATO Lecture on "Passive Radar Imaging" of the Lecture Series SET-243 on Passive Radar.

1.0 INTRODUCTION

Radar Imaging refers to the ability to form images of natural or man-made objects using Electro-Magnetic echo location. As will become clearer later, coherent radars may have suitable specifications that allow implementation of special features using specific signal processing. We may argue that, given a suitable coherent radar, radar imaging can be provided by adding some "special" signal processing to the received signal. Conventional radar images are typically represented as two-dimensional (2D) images where a mapping function transforms the three-dimensional (3D) world into a 2D image. An obvious comparison could be formulated with photographic images, as these are also the result of some mapping from the 3D world into a 2D photographic image. However, there are several differences that may be pointed out in regards of the type of mapping and image features. Radar images, as well as other type of images (e.g. photographic, infra-red, X-ray images) are usually characterised by means of some quality features, such as geometrical and radiometric resolution and signal-to-noise (SNR) ratio.

Pushed by the need to form high quality radar images that can be used in applications such as automatic target recognition and classification, researchers have designed a variety of radar imaging processors. In this paper we will introduce the fundamental concepts at the base of radar imaging and we will provide an overview of the most commonly used radar imaging techniques, with particular emphasis on passive radar imaging. Examples will be also used throughout this chapter to clarify concepts and to show some radar imaging results.

2.0 HISTORICAL OVERVIEW

We have to distinguish two starting points when considering the origins of radar imaging: one for Synthetic Aperture Radar (SAR) and one for Inverse Synthetic Aperture Radar (ISAR). Although the two approaches to radar imaging have quite a lot in common, there are some significant differences that mark a line between them. As mentioned in [1], the SAR concept was conceived in 1951 by Carl Wiley, although the first operational system (classified) was built in 1957 by the Willow Run Laboratories of the University of Michigan for the US Department of Defense (DoD). Unclassified SAR systems were successfully built by NASA in the 1960s. The first spaceborne SAR system, SEASAT-A, was launched in 1978. Although this spaceborne system was specifically designed for oceanographic purposes, it also produced important results in other fields, such as in ice and land studies. The results obtained with SEASAT-A demonstrated the importance of radar imaging for the observation of the earth. Since then, several spaceborne SAR systems have been launched that provide improved resolution, wider coverage and faster revisit times. Several airborne SAR systems have also been developed to overcome limitations of spaceborne SAR systems, such as cost,

revisiting time and resolution. After the first experiments on the 1960s operated by the NASA, other important missions have been accomplished, such as the SIR-A, SIR-B and SIR-C missions, which flew in 1981, 1984 and 1994, respectively. The history of ISAR began later, when Walker and Aushermann, with their pioneering work [2, 3] introduced the concept of radar imaging of rotating objects with fixed antennas. The main insight in their work was to exploit Doppler information generated by the rotation of an object to separate echoes returning from different parts of the object along a cross-range axis. Such Doppler separation, together with the time-delay separation (along the radar range), produces a two-dimensional (2D) image, which can be mapped onto an image plane.

3.0 INVERSE SYNTHETIC APERTURE RADAR

The concept of Inverse Synthetic Aperture Radar will be introduced in a modern way. Rather than traditionally considering an ISAR system as a configuration where the radar is static and on object moves with respect to it, we will migrate from the SAR concept and geometry.

3.1 From SAR to ISAR

Real aperture antennas or antenna arrays do not provide a viable solution for radar imaging systems. Nevertheless, high cross-range resolution can only be enabled if an antenna aperture can be formed. The first idea of SAR was conceived by thinking of a single element that moves along a given trajectory, therefore providing the means for forming a virtual array in a given time interval. Such concept is depicted in Fig. 3.1, where a synthetic array formation is compared with a real array. As the formation of the synthetic aperture is not instantaneous, any equivalence between a synthetic aperture and a real array can be stated only if the illuminated scene is static during the synthetic aperture formation (from t_1 to t_N).
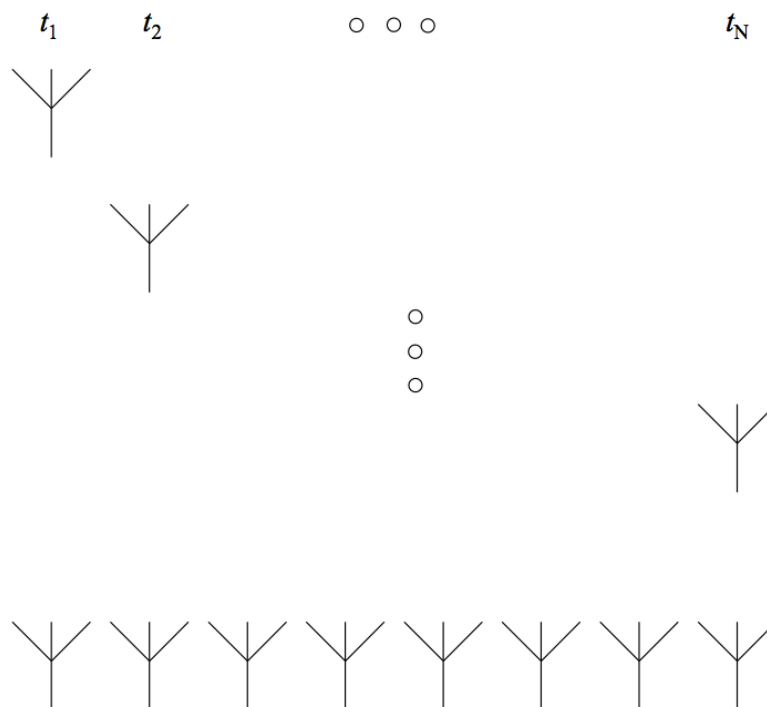

Figure 3.1. Synthetic Aperture - Virtual array

If such an assumption can be made, there would be no physical difference between the signal acquired by a synthetic aperture radar and a real aperture radar (which makes use of a real array). The condition under which the effect of the element motion can be neglected is known as the stop & go assumption, which implies that the transmission of the signal and the reception of its echo occur instantaneously at a particular position. Obviously, this assumption cannot be perfectly matched unless the platform that carries the radar stops every time a pulse is transmitted and received before moving to the next position. Nevertheless, in practical scenarios, such an assumption can be considered satisfied since the round-trip delay (the time for the e.m. wave to propagate from the radar to the illuminated scene and back) is short enough to neglect the element offset created by the platform motion during such a time interval.
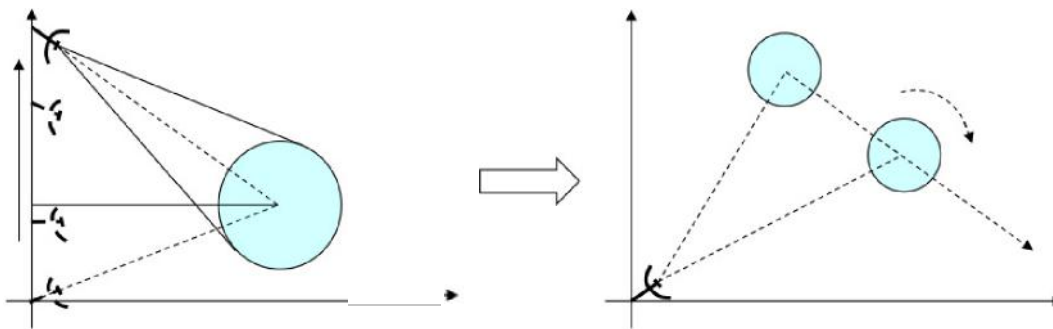

Figure 3.2. From Spot-light SAR to ISAR

Attention should now be paid to the "relative motion" that there is between the platform and the target, as such a motion is not necessarily produced by a moving platform that carries the radar. Relatively speaking, if the sensor is stationary and the target moves with respect to it inducing a relative motion, a synthetic aperture would be created at the same way. To strengthen this concept, one could argue that the cases of stationary target and moving platform and the case of stationary platform and moving target can only be stated once the reference system has been chosen. In fact, by placing the reference system on the target, the first case is enabled whereas, by placing the reference system on the radar, the latter is obtained. According with this last view, the differences between synthetic aperture and inverse synthetic aperture would only depend on where the reference system is positioned. Such a concept is depicted in Fig. 3.2 where a Spot-light SAR configuration is transformed into an ISAR configuration by moving the reference system from the target to the radar.

Conversely, the same concept may be argued by starting with a controlled ISAR configuration such as that of a turntable experiment. In a turntable configuration, the antenna is fixed on the ground (typically mounted on a turret) and the target is positioned on a turntable, which rotates as the radar takes measurements of the target. By moving the reference system from the radar to the target, a circular SAR geometry can be enabled, as depicted in Fig. 3.3.
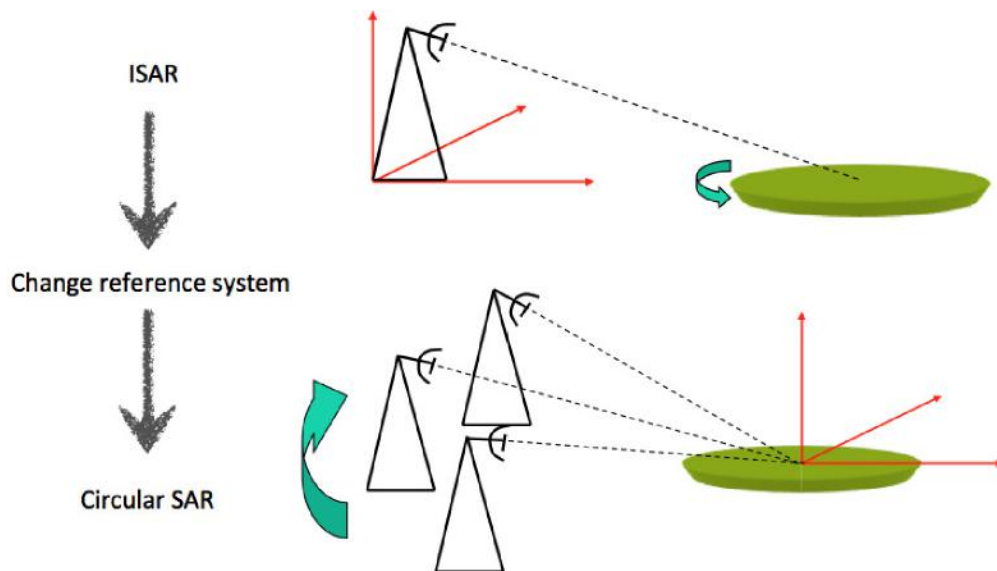
Figure 3.3. From ISAR to Circular SAR

In truth, a subtle but significant detail exists that substantially defines the difference between SAR and ISAR. Such a detail is the cooperation of the illuminated target. To better explain this concept, one may place the reference system on the target. If such a target moves (with unknown motions) with respect to the radar, the synthetic aperture formed during the Coherent Processing Interval (CPI) differs from the expected one (which is formed by controlled platform motion). Any SAR image formation that follows would be then based on the erroneously predicted synthetic aperture and therefore would lead to defocussed images. A pictorial example is shown in Fig. 3.4.
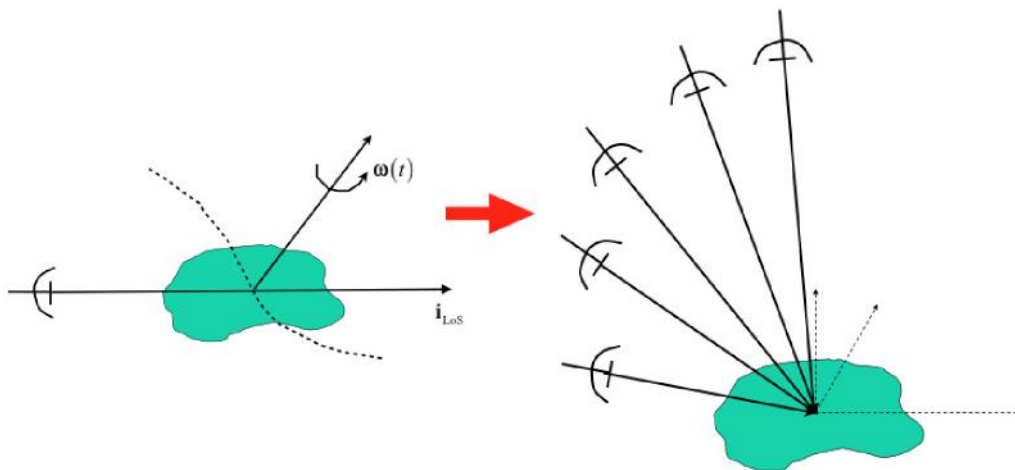

Figure 3.4. Synthetic array formed by a non-cooperative target

4.0 PASSIVE RADAR IMAGING

Passive bistatic radars (PBR) have recently received a great deal of interest from the scientific community [4–6]. This is because passive radar systems have a number of obvious advantages over active radar systems (low cost, reduced electromagnetic pollution, low vulnerability to electronic countermeasure and counter-stealth

advantage), but also because of the recent technological advances that have made the realization of low cost passive coherent location (PCL) systems and real-time processing possible [7–9]. Illuminators of opportunity (IOs), which are used as electromagnetic sources for PCL systems, may be of different types. Typically, IOs are classified as either external dedicated radar systems or other types of illuminators, such as communications transmitters. The latter are of great interest as they allow 1) large areas to be covered, 2) a wide range of frequencies to be used (which typically are not available to radar systems), and 3) signals to be acquired continuously. It should be mentioned that, although the principle under which PBR works is independent of the transmitted waveform, the achievable performance (e.g. spatial resolutions) depends on the waveform and therefore they may change according to the available IO.

As research in this field progresses, more radar techniques are added to PCL systems to make PBR able to handle several tasks and to be applied to different scenarios. One such scenario is radar imaging of non-cooperative targets through inverse synthetic aperture radar (ISAR) imaging, which, in turn, may open the doors to non-cooperative target recognition (NCTR) capabilities. Some studies have been carried out in the recent past that relate to this research field [10–15]. However, [10–12] mainly refer to synthetic aperture radar (SAR) imaging by exploiting communications transmitters. Therefore, the problem of how to obtain a well-focused image of a non-cooperative moving target is not addressed in these papers. The imaging problem in a passive multi-static scenario is formulated as a detection problem in [14, 15]. Specifically, the method relies on a test of binary hypothesis that is used to estimate both the target's position and its velocity. Even if the authors demonstrate its feasibility by using simulated data, it is not suited for the case of distributed targets. Finally, a GSM (Global System for Mobile communications) based PBR is used in [13] to detect and image non-cooperative moving targets. However, this paper does not provide any theoretical formulation of the passive radar imaging problem and does not extend to other types of IOs.

Very recently, some work has been carried out in [15–17] that has demonstrated that Passive Bistatic ISAR (PB-ISAR) imaging is viable by using PBR systems. In these papers, the concept of PB-ISAR has been defined and its feasibility has been demonstrated. Specifically, in [15–17], a PB-ISAR algorithm has been proposed based on two main concepts. The first one concerns the bistatic ISAR theory. Owing to the fact that a passive radar is intrinsically bistatic (this is because the transmitter and the receiver are not collocated), the bistatic ISAR theory can be applied in this framework. The second concept concerns the application of ISAR processing to unfocused range-Doppler images of moving targets. As demonstrated in [18], ISAR imaging can be used to refocus SAR images of moving targets. The application of ISAR processing to unfocused SAR images of moving targets was demonstrated to be viable after projecting the unfocused image back to the wavenumber domain. As a SAR image of a moving target may be approximated as an unfocused range-Doppler image, this becomes perfectly equivalent to what happens when forming range-Doppler maps of moving targets with a PBR system [16]. Due to this analogy, the same processing proposed in [18] can be used in the framework of PB-ISAR. The authors however did not provide any mathematical proof of it in [16], and they did not show how data suitable for the application of ISAR processing can be obtained from a range-Doppler map.

4.1   Mathematical Aspects of Passive ISAR imaging

As stated in the Introduction and detailed in [15–17], a PB-ISAR algorithm has been proposed and its effectiveness has been proven by using simulated and real data. The input of the PB-ISAR algorithm is a range-Doppler map. After the target detection step, the range-Doppler image of the target of interest is extracted by selecting a rectangular window in the range-Doppler map, which contains mainly the target's echo plus a little amount of clutter and noise. The selected part of the range-Doppler map is the input of the ISAR processing. However, ISAR processors are typically designed to work either in the frequency/slow-time domain or in the range/slow-time domain. Therefore, the available data in the range-Doppler domain should be suitably transformed into one of the above-mentioned domains. The main object of this subsection is to demonstrate that data in the frequency/slow-time domain can be obtained by inverse Fourier transforming the range-Doppler image of the target.

4.1.1 Mathematical Background

Let the geometry be represented by Fig. 4.1 where T_x (x_1, x_2, x_3) is a Cartesian reference system embedded on the target, T_ξ (ξ_1, ξ_2, ξ_3) is a Cartesian reference system centred on the transmitter, and R_{TxTg}, R_{TxRx}, R_{RxTg} represent the transmitter-target, transmitter-receiver, and receiver-target distances. The receiver is composed of two antennas, namely, the reference antenna A_{ref} , which points towards the transmitter to acquire the reference signal $s_{ref}(t)$, and the surveillance antenna A_{surv}, which points towards the target to acquire the surveillance signal $s_{surv}(t)$. As already stated, a passive radar is intrinsically bistatic, since the transmitter and the receiver are typically not co-located. As shown in [20] a bistatic configuration can be approximated with an equivalent monostatic configuration with a virtual sensor located along the bisector of the bistatic angle β and at a distance from the target which is the semi-sum of the distances R_{RxTg} and R_{TxTg}. Therefore, a bistatic equivalent monostatic (BEM) radar can be defined as shown in Fig. 4.1 and the bistatic ISAR theory [19] can be applied to this framework.
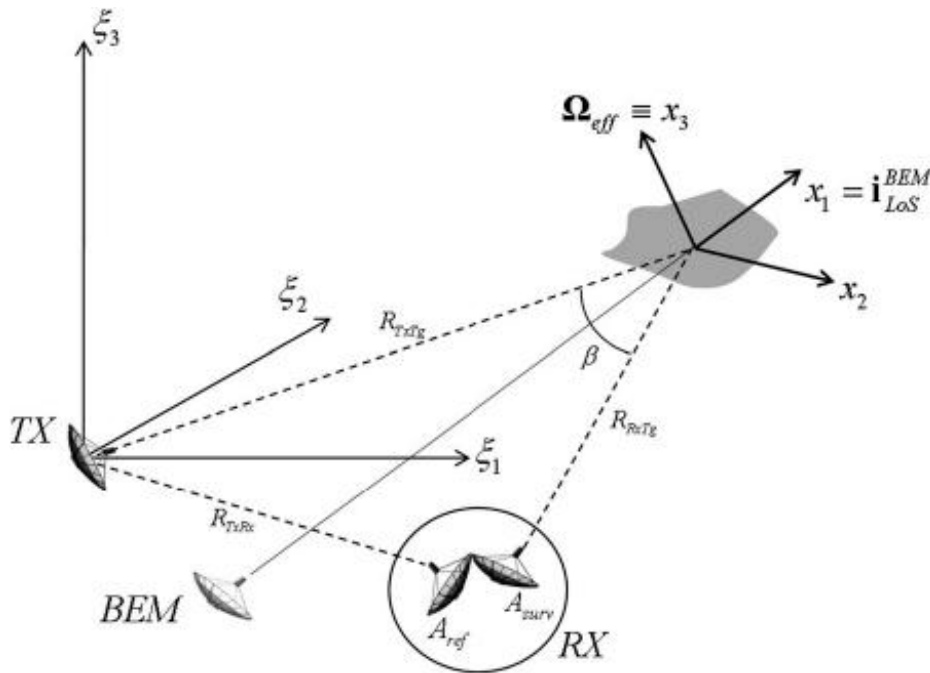

Figure 4.1 – Bistatic ISAR Geometry

The target angular motion with respect to the BEM radar can be described by means of the total target angular rotation vector $\Omega_T(t)$. The effective rotation vector $\Omega_{eff}(t)$ is the rotation vector component that contributes to the synthetic aperture formation. This latter can be obtained from the total target rotation vector by applying a vector product, specifically,

$$\mathbf{\Omega}_{eff}(t) = \mathbf{i}_{LoS}^{BEM} \times \left[\mathbf{\Omega}_T(t) \times \mathbf{i}_{LoS}^{BEM} \right]$$

(1)

where $\mathbf{i}_{LoS}^{BEM}$ is the unit vector which identifies the BEM radar line of sight. As shown in [20], the cross-ambiguity function between the surveillance signal $s_{surv}(t)$ and the reference signal $s_{ref}(t)$ can be seen as a weighted sum of the ambiguity functions calculated within each batch. Specifically, when $T_b v_{max}, << 1$, where T_b is the batch interval and v_{max} is the maximum allowed Doppler frequency, the cross-ambiguity function can be written as follows:

$$\chi(\tau, \nu) = \sum_{n=1}^{N_b} e^{-j2\pi\nu nT_b} \cdot \int s_s(t; n) s_r^*(t - \tau; n) \, dt$$

(2)

where

$$s_r(t, n) = s_{ref}(t + nT_b) \cdot rect\left(\frac{t - T_b/2}{T_b}\right)$$

(3a)

$$s_s(t, n) = s_{surv}(t + nT_b) \cdot rect\left(\frac{t - (T_b + \tau_{max})/2}{T_b + \tau_{max}}\right)$$

(3b)

$t \in [0, T_{int}]$, T_{int} is the integration time, n is the batch number, and τ_{max} is the maximum allowed delay-time, which is directly related to the maximum target distance.
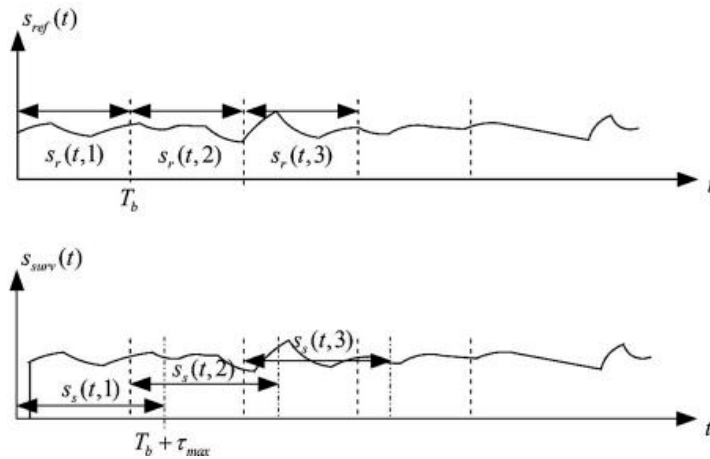

Fig. 4.2. Graphical representation of both surveillance signal $s_{surv}(t)$ and reference signal $s_{ref}(t)$.

The reference signal $s_{ref}(t)$ is modelled as the sum of N_b contiguous batches of length T_b

$$s_{ref}(t) = \sum_{n=1}^{N_b} s_r(t - nT_b, n)$$

(4)

Since the target distance is not known a priori and in order to guarantee the maximum integration gain at the output of each cross-correlation, $s_{surv}(t)$ is divided into partially overlapped batches in the integration time, as shown in (5).

$$s_{surv}(t) = \sum_{n=1}^{N_b} s_s(t - nT_b, n)$$

(5)

For the sake of clarity both $s_{ref}(t)$ and $s_{surv}(t)$ are graphically represented in Fig. 4.2.

Equation (1) can then be reformulated as follows:

$$\chi(\tau, \nu) = \sum_{n=1}^{N_b} e^{-j2\pi\nu nT_b} \cdot \chi_{cc}(\tau, n)$$

(6)

where

$$\chi_{cc}(\tau, n) = \int s_s(t, n) s_r^*(t - \tau, n) \, dt \tag{7}$$

represents the cross-ambiguity function relative to the nth block. The cross-correlation in (7) implements the matched filter and therefore the pulse compression. It is therefore straightforward to conclude that $\chi_{cc}(\tau, n)$ represents the range profile relative to the nth block.

4.1.2   Signal Modelling

The objective of this section it to prove that by inverse Fourier transforming along both the delay-time τ, and the Doppler frequency v, a frequency/slow-time data that is suitable for the application of ISAR processing can be obtained. Equation (6) highlights that the cross-ambiguity function is the Fourier series of $\chi_{cc}(\tau, n)$. Therefore by inverse Fourier transforming (6) with respect to the variable v, the range profile history $\chi_{cc}(\tau, n)$ is derived (one range profile for each slow-time n).

$$\chi_{cc}(\tau, n) = FT^{-1}\left[\chi(\tau, \nu)\right] \tag{8}$$

The signal backscattered by the target, that is, $s_{surv}(t)$, can be written as follows:

$$s_{surv}(t) = \iiint_V g(\mathbf{x}) s_{ref}\left(t - \tau(t; \mathbf{x})\right) d\mathbf{x} \tag{9}$$

Where $\tau(t; \mathbf{x}) = \frac{R(t; \mathbf{x})}{c}$, $R(t; \mathbf{x})$ is the bistatic distance between an arbitrary point on the target, the receiver, and the transmitter; $\mathbf{x}$ is the vector locating the point of the target in the coordinates system embedded on the target; c is the light speed in vacuum; V is the spatial domain where the target's reflectivity function $g(\mathrm{x})$ is defined. In a real scenario, the surveillance signal is also affected by multipath, which is often modelled as an additive signal. Multipath is usually taken care of by pre-processing the data. This step is necessary also for more basic radar applications such as target detection and tracking [22–23]. In the following sections, it is assumed that the surveillance signal has been pre-processed to reduce the multipath and therefore it is neglected. By assuming the target stationary during the batch interval T_b, the delay-time can be approximated as $\tau_{\mathbf{x}}(t; \mathbf{x}) \simeq \tau_{\mathbf{x}}(n; \mathbf{x})$. Therefore, by exploiting (4), (9) can be reformulated as shown in (10).

$$s_{surv}(t) = \sum_{n=1}^{N_b} \iiint_V g(\mathbf{x}) s_r\left(t - \tau_{\mathbf{x}}(n; \mathbf{x}) - nT_b, n\right) d\mathbf{x} \tag{10}$$

As mentioned above, in order to have the same integration gain at each batch, the surveillance signal is divided into batches of length $T_b + \tau_{\max}$. Then the nth batch of $s_{surv}(t)$ can be written as in (11):

$$s_s(t, n) = \iiint_V g(\mathbf{x}) \left[s_r\left(t - \tau_{\mathbf{x}}(n; \mathbf{x}) - nT_b, n\right) \cdot rect\left(\frac{t - (T_b + \tau_{\mathbf{x}}(n; \mathbf{x}))/2}{T_b}\right) + s_{sn}(t, n; \mathbf{x}) \right] d\mathbf{x} \tag{11}$$

where $s_{sn}(t, n; \mathbf{x})$ is a portion of the surveillance signal in the adjacent batch, and is defined as follows:

$$s_{sn}(t, n; \mathbf{x}) = s_{surv}(t + nT_b) rect\left(\frac{t - (T_b + \tau_{\mathbf{x}}(n; \mathbf{x}) + (\tau_{max} - \tau_{\mathbf{x}}(n; \mathbf{x}))/2)}{\tau_{max} - \tau_{\mathbf{x}}(n; \mathbf{x})}\right) \tag{12}$$

By using (11), (7) can be rewritten as follows:

$$\chi_{cc}(\tau, n) = \chi_{cc}^s(\tau, n) + \sigma_{cc}(\tau, n) \tag{13}$$

The contribution $\chi_{cc}^{s}(\tau, n)$ is larger than $\sigma_{cc}(\tau, n)$, as the signals in different batches are typically uncorrelated. In any case, even when a small correlation exists, $\sigma_{cc}(\tau, n)$ can be neglected as its average is much smaller than the average of $\chi_{cc}^{s}(\tau, n)$. Therefore $\sigma_{cc}(\tau, v)$ can be neglected as shown in (14):

$$\chi_{cc}(\tau, n) \simeq \chi_{cc}^{s}(\tau, n) = \iiint_{V} g(\mathbf{x}) \int_{t} s_r(t - \tau(n; \mathbf{x})) s_r^*(t - \tau, n) dt d\mathbf{x}$$

(14)

By Fourier transforming $\chi_{cc}(\tau, n)$ with respect to the delay-time domain, the signal $\chi_{cc}(f, n)$ in the frequency/slow-time domain is obtained as follows:

$$X_{cc}(f, n) = FT[\chi_{cc}(\tau, n)]$$
$$= \iiint_{V} g(\mathbf{x}) \int_{t} s_r(t - \tau(n; \mathbf{x}), n) \int_{\tau} s_r^*(t - \tau, n) e^{-2j\pi\tau f} d\tau \; dt \; d\mathbf{x}$$
$$= \iiint_{V} \int_{t} s_r(t - \tau(n; \mathbf{x}), n) S_r^*(f, n) e^{-j2\pi ft} dt \; d\mathbf{x}$$
$$= \iiint_{V} g(\mathbf{x}) S_r^*(f, n) S_r(f, n) e^{-j2\pi f\tau(n; \mathbf{x})} d\mathbf{x}$$
$$= |S_r(f, n)|^2 \iiint_{V} g(\mathbf{x}) e^{-j2\pi f\tau(n; \mathbf{x})} d\mathbf{x}$$

(15)

where $S_r(f, n)$ is the Fourier transform of $s_r(\tau, n)$.

The delay-time relative to an arbitrary scatterer can be written as follows:

$$\tau_{\mathbf{x}}(n; \mathbf{x}) = \frac{R_{\mathbf{x}}(n)}{c} = \frac{(R_{T\mathbf{x}}(n) + R_{R\mathbf{x}}(n))}{c}$$

(16)

where $R_{Tx}(n)$ and $R_{Rx}(n)$ are the distances between an arbitrary scatterer and the transmitter and the receiver, respectively. When the target size is much smaller than both the target-transmitter and target-receiver distances, the straight-iso-range approximation can be applied, therefore both R_{Tx} and R_{Rx} can be approximated as shown subsequently:

$$R_{T\mathbf{x}}(n) = R_{T0}(n) + \mathbf{x} \cdot \mathbf{i}_{LoS,T}(n)$$
$$R_{R\mathbf{x}}(n) = R_{R0}(n) + \mathbf{x} \cdot \mathbf{i}_{LoS,R}(n)$$

(17)

where R_{T0} and R_{R0} are the distances between an arbitrary point 0 on the target and the transmitter and the receiver,

$$\tau(n; \mathbf{x}) = \frac{2}{c} \left[R_{B,0}(n) + K(n)\mathbf{x} \cdot \mathbf{i}_{LoS,B}(n) \right]$$

(18)

Where

$$R_{B,0}(n) = \frac{R_{T0}(n) + R_{R0}(n)}{2}$$

$$K(n) = \left| \frac{\mathbf{i}_{LoS,T}(n) + \mathbf{i}_{LoS,R}(n)}{2} \right| = cos\left(\frac{\beta(n)}{2}\right)$$

$$\mathbf{i}_{LoS,B}(n) = \frac{\mathbf{i}_{LoS,T}(n) + \mathbf{i}_{LoS,R}(n)}{|\mathbf{i}_{LoS,T}(n) + \mathbf{i}_{LoS,R}(n)|}$$

(19)

where $\beta(n)$ represents the value of the bistatic angle at time n (see Fig. 4.1 for the geometrical interpretation of β). Equation (15) can then be rewritten as follows:

$$X_{cc}(f,n) = |S_r(f,n)|^2 \, e^{-j4\pi\frac{f}{c}R_{B,0}(n)} \iiint_V g(\mathbf{x}) e^{-j4\pi\frac{f}{c}K(n)\mathbf{x}\cdot\mathbf{i}_{LoS,B}(n)} \, d\mathbf{x}$$

(20)

4.1.3 PB-ISAR Imaging

The PB-ISAR imaging algorithm proposed in this paper is based on the image contrast-based autofocus (ICBA) algorithm and the range-Doppler technique. The ICBA algorithm is a parametric technique and it is based on image contrast (IC) maximization, whose details can be found in [24]. The range-Doppler technique [2] is based on the assumption that the Doppler frequency of each scatterer, relative to a reference point taken on the target, is constant within the observation time. This assumption is usually satisfied when the effective rotation vector $\Omega_{eff}(t)$ can be assumed constant within the observation time. Let $\theta(n)$ be the target aspect angle at the nth block with respect to the BEM radar, the scalar product $\mathbf{x}\cdot\mathbf{i}_{LoS,B}(n)$ can be reformulated as in (21):

$$\mathbf{x} \cdot \mathbf{i}_{LoS,B}(n) = x_1 cos(\theta(n)) + x_2 sin(\theta(n))$$

(21)

where x_1 and x_2 are the scatterer coordinates in the image projection plane (IPP), that is the plane orthogonal to the effective rotation vector Ω_{eff}. For notation simplicity, and as can be noted in Fig. 4.1, the reference system embedded on the target T_x has been chosen so that the two-dimensional plane (x_1, x_2) coincides with the ISAR IPP.

$$X_{cc}(f,n) = |S_r(f,n)|^2 \, e^{-j4\pi\frac{f}{c}R_{B,0}(n)} \iiint_V g(\mathbf{x}) e^{-j2\pi[x_1 X_1(f;n) + x_2 X_2(f,n)]} d\mathbf{x}$$

(22)

Where

$$X_1(f,n) = \frac{2fK(n)cos(\theta(n))}{c}$$

$$X_2(f,n) = \frac{2fK(n)sin(\theta(n))}{c}$$

(23)

The variation of the distance between the target and the BEM, namely $R_{B,0}(n)$, within the observation time, causes a range migration that must be accounted for. In order to compensate the target radial motion, the phase term $e^{-j4\pi\frac{f}{c}R_{B,0}(n)}$ outside the sum in (22), must be estimated and removed. In ISAR scenarios, where the target is usually non-cooperative, this operation is performed by means of autofocusing

algorithms. The estimation of the term $e^{-j4\pi\frac{f}{c}R_{B,0}(n)}$ resorts to the estimation of $R_{B,0}(n)$ and therefore to the target radial motion parameters.

After a perfect radial motion compensation, the signal $X'_{cc}(f,n)$ can be expressed as in (24):

$$X'_{cc}(f,n) = W(f,n) \int_{x_1} \int_{x_2} g'(x_1,x_2)e^{-j2\pi[x_1 X_1(f,n)+x_2 X_2(f,n)]}dx_1\ dx_2$$

$$= W(f,n)G'\left(X_1(f,n),X_2(f,n)\right) \tag{24}$$

where $W(f,n)$ represents the support band of $X_{cc}(f,n)$, that is the region in the (f, n) domain where the signal Xcc (f, n) exists and it is expressed by (25):

$$W(f,n) = |S_r(f,n)|^2 \cdot \mathcal{R}(n) \tag{25}$$

where $\mathcal{R}(n) = rect(n) = u(n) - u(n - N_b)$, $u(n)$ is the unit step discrete function, $N_b = \left\lfloor \frac{T_{int}}{T_b} \right\rfloor$, $g'(x_1,x_2) = \int_{x_3} g(\mathbf{x})dx_3$ is the projection of the target reflectivity function onto the IPP, and $G'(X_1,X_2) = 2D - FT\left[g'(x_1,x_2)\right]$, that is G' (X_1, X_2) is the two-dimensional Fourier transform of $g'(x_1, x_2)$. An estimate of $g'(x_1, x_2)$ can be then obtained by inverse Fourier transforming $X'_{cc}(f,n)$.

Under the hypotheses that the aspect angle variation within the integration time is such that $|\theta(n)| \ll 1$, and that the bistatic angle changes are relatively small ($\beta(n) \sim \beta_0$), both the spatial frequencies X_1 (f, n) and X_2 (f, n) defined in (23), can be approximated as follows [19]:

$$X_1(f,n) \simeq X_1(n) = \frac{2fK_0}{c}$$

$$X_2(f,n) \simeq X_2(f) = \frac{2f_0 K_0 \theta(n)}{c} = \frac{2f_0 K_0 \Omega_{eff}t}{c} \tag{26}$$

where $K_0 \simeq cos\frac{\beta_0}{2}$ [19].

By substituting both X_1 (f) and X_2 (n) in (24), $X'_{cc}(f,n)$ can be rewritten as follows:

$$X'_{cc}(f,n) = W(f,n) \int_{x_1} \int_{x_2} g'(x_1,x_2)e^{-j2\pi\left[x_1\frac{2fK_0}{c}+x_2\frac{2f_0 K_0 \Omega_{eff}t}{c}\right]}dx_1\ dx_2 \tag{27}$$

By substituting the variables (x_1, x_2) with the variables (τ, v), as shown in (28)

$$\nu = \frac{2f_0 K_0 \Omega x_2}{c}$$

$$\tau = \frac{2x_1 K_0}{c} \tag{28}$$

(27) can be reformulated as follows:

$$X'_{cc}(f,n) = C \cdot W(f,n) \int_{\nu} \int_{\tau} g'(\tau,\nu)e^{-j2\pi[\nu t+\tau f]}d\nu\ d\tau \tag{29}$$

Where

$$C = \frac{c^2}{4 f_0 K_0^2 \Omega_{eff}}$$

By observing (28), it can be noted that both range and cross-range resolutions are degraded by a factor K_0 with respect to those achievable with a monostatic radar. By applying the range-Doppler technique to the signal in (29), the ISAR image of the target is obtained

$$\chi_{cc}(\tau, \nu) = C \cdot w(\tau, \nu) \otimes \otimes g'(\tau, \nu) \tag{30}$$

where $w(\tau, \nu)$ represents the point spread function (PSF) of the ISAR system in the delay-time/Doppler domain, which depends on both the spectral content of the reference signal and on the integration time. The symbol $\otimes \otimes$ indicates double convolution, which is defined in (31).

$$\chi_{cc}(\tau, \nu) = C \cdot \int_{\alpha=-\infty}^{+\infty} \int_{\beta=-\infty}^{+\infty} w(\alpha, \beta) \cdot g'(\tau - \alpha, \nu - \beta) \ d\alpha d\beta \tag{31}$$

For the sake of clarity, a block scheme of the algorithm is shown in Fig. 4.3, where a PB-ISAR processing chain is developed for each detected target of interest and the ISAR algorithm step consists of both autofocus and image formation. It is quite important to remark that the results obtained in this section are independent of the IO and therefore independent of the reference signal waveform.

More details may be found in [25-27] whereas a number of examples of Passive ISAR images are provided with the lecture presentation slides.
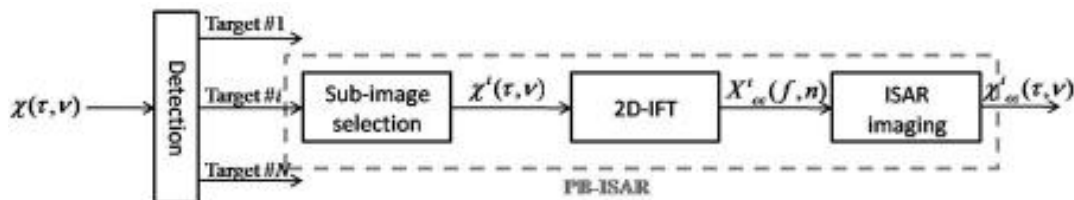

Figure 4.3. PB-ISAR algorithm flow chart.

5.0 CONCLUSIONS

Passive ISAR provides the ability to form 2D radar images of non-cooperative targets for passive radar. This specific signal processing may enable classification capabilities also in passive radar if databases and classification procedures are created for this type of radar, which makes use of bistatic configurations, low frequencies and non-radar-specific waveforms.

6.0 REFERENCES

[1] G. Franceschetti, R. Lanari, *Synthetic Aperture Radar Processing*, CRC Press, 1999.

[2] J.L.Walker, *Range-doppler imaging of rotating objects*, IEEE Trans. Aerosp. Electron. Syst. 16 (1980) 23–52.

[3] D.A. Ausherman, A. Kozma, J.L. Walker, H.M. Jones, E.C. Poggio, *Developments in radar imaging*, IEEE Trans. Aerosp. Electron. Syst. 20 (1984) 363–400.

[4] Melvin, W. L., and Scheer, J. A., *Principles of Modern Radar: Advances Techniques*. Raleigh, NC: SciTech Publishing, 2012.

[5] Howland, P., *Editorial: Passive radar systems*, IEE Proceedings-Radar, Sonar and Navigation, 152 (June 2005), 105–106.

[6] Farina, A., and Kuschel, H., *Special Issue on Passive Radar (Part I)*, IEEE Aerospace and Electronic Systems Magazine, 27, 10 (2012).

[7] Malanowski, M., Mazurek, G., Kulpa, K., and Misiurewicz, J., *FM based PCL radar demonstrator*, In Proceedings of the International Radar Symposium, 2007.

[8] O'Hagan, D., Kuschel, H., Ummenhofer, M., Heckenbach, J., and Schell, J., *A multi-frequency hybrid passive radar concept for medium range air surveillance*, IEEE Aerospace and Electronic Systems Magazine, 27 (Oct. 2012), 6–15.

[9] Cetin, M., and Lanterman, A. D., *Region-enhanced passive radar imaging*, IEE Proceedings-Radar, Sonar and Navigation, 152, 3 (2005), 185–194

[10] Garry, J., Baker, C., Smith, G., and Ewing, R., *Doppler imaging for passive bistatic radar*, In IEEE Radar Conference 2013, 2013.

[11] Wang, L., Yarman, C. E., and Yazici, B., *Theory of passive synthetic aperture radar*, In Excursions in Harmonic Analysis, Vol. 1 (Applied and Numerical Harmonic Analysis Series) New York: Springer-Birkhauser, 2013

[12] Krysik, P., Kulpa, K., Samczynski, P., Szumski, K., and Misiurewicz, J., *Moving target detection and imaging using GSM-based passive radar*, In IET International Conference on Radar Systems (Radar 2012), 2012, pp. 1–4

[13] Wang, L., and Yazici, B., P*assive imaging of moving targets exploiting multiple scattering using sparse distributed apertures*, *Inverse Problems*, 28, 12 (2012)

[14] Wang, L., and Yazici, B., *Passive imaging of moving targets using sparse distributed apertures*, *SIAM Journal on Imaging Sciences*, 5, 3 (2012), Page(s) 769–808

[15] Olivadese, D., Giusti, E., Petri, D., Martorella, M., Capria, A., and Berizzi, F., *Passive ISAR with DVB-T signals*, IEEE Transactions on Geoscience and Remote Sensing, 51, 8 (2013), 1–10

[16] Olivadese, D., Giusti, E., Petri, D., Martorella, M., Capria, A., and Berizzi, F., and Soleti, R., *Passive ISAR imaging of ships by using DVB-T signals*, In Radar 2012, International Conference on Radar Systems

[17] Olivadese, D., Martorella, M., Giusti, E., Petri, D., and Berizzi, F., *Passive ISAR with DVB-T signal*, 9th European Conference on Synthetic Aperture Radar, 2012 (EUSAR), Apr. 2012, pp. 287–290

[18] Martorella, M., Giusti, E., Berizzi, F., Bacci, A., and Mese, E. D., *ISAR based technique for refocussing non-cooperative targets in SAR images*, IET Radar, Sonar, Navigation, 6 (May 2012), 1–9

[19] Martorella, M., Palmer, J., Homer, J., Littleton, B., Longstaff, I. D., *On bistatic inverse synthetic aperture radar*, IEEE Transactions on Aerospace and Electronic Systems, 43, 3 (2007), 1125–1134

[20] Petri, D., Moscardini, C., Martorella, M., Conti, M., Capria, A., and Berizzi, F., *Performance analysis of the batches algorithm for range-Doppler map formation in passive radar*, In Proceedings of the International Conference on Radar Systems (RADAR 2012).

[21] Colone, F., Cardinali, R., and Lombardo, P., *Cancellation of clutter and multipath in passive radar using a sequential approach*, In 2006 IEEE Conference on Radar, Apr. 2006, p. 7.

[22] Haykin, S., *Adaptive Filtering Theory*. Upper Saddle River, NJ: Prentice-Hall, 2002

[23] Zhao, Z., Wan, X., Shao, Q., Gong, Z., and Cheng, F., *Multipath clutter rejection for digital radio mondiale-based HF passive bistatic radar with OFDM waveform*, IET Radar, Sonar Navigation, 6 (Dec. 2012), 867–872

[24] Martorella, M., Berizzi, F., and Haywood, B., *A contrast maximization based technique for 2D ISAR autofocusing*, IEE Proceedings-Radar, Sonar and Navigation, 152, 4 (2005), 253–262

[25] Martorella M., Giusti E., *Theoretical Foundation of Passive ISAR*, IEEE Transactions on Aerospace and Electronic Systems, Vol. 50, No. 3, July 2014, Pages: 1701-1714

[26] V. C. Chen, M. Martorella, "Inverse Synthetic Aperture Radar Imaging: Principles, Algorithms and Applications", IET/Scitech Publishing, 2014

[27] F. Berizzi, M. Martorella, E. Giusti, "Radar Imaging for Maritime Observation", CRC Press, Taylor and Francis, 2016